Journal Article

Thin CdTe layers deposited by a chamberless inline process using MOCVD, simulation and experiment

Monir, S., Kartopu, G., Barrioz, V., Lamb, D., Irvine, S.J.C., Yang, X. and Vagapov, Y.

applied sciences

MDPI

Article

Thin CdTe Layers Deposited by a Chamberless Inline Process using MOCVD, Simulation and Experiment

Shafiul Monir [1], Giray Kartopu [2], Vincent Barrioz [3], Dan Lamb [2], Stuart J. C. Irvine [2], Xiaogang Yang [4] and Yuriy Vagapov [1,*]

1 Faculty of Art, Science and Technology, Wrexham Glyndwr University, Plas Coch, Mold Road, Wrexham LL11 2AW, UK; s.monir@glyndwr.ac.uk
2 Centre for Solar Energy Research, College of Engineering, Swansea University, OpTIC Centre, St. Asaph Business Park, St. Asaph LL17 0JD, UK; giray.kartopu@swansea.ac.uk (G.K.); d.a.lamb@swansea.ac.uk (D.L.); s.j.c.irvine@swansea.ac.uk (S.J.C.I.)
3 Department of Mathematics, Physics and Electrical Engineering, Northumbria University, Ellison Building, Newcastle Upon Tyne NE1 8ST, UK; vincent.barrioz@northumbria.ac.uk
4 Faculty of Science and Engineering, University of Nottingham Ningbo, Sir Peter Mansfield Building, 199 Taikang East Road, Ningbo 315100, China; xiaogang.yang@nottingham.edu.cn
* Correspondence: y.vagapov@glyndwr.ac.uk

Received: 14 December 2019; Accepted: 11 February 2020; Published: 3 March 2020

Abstract: The deposition of thin Cadmium Telluride (CdTe) layers was performed by a chamberless metalorganic chemical vapour deposition process, and trends in growth rates were compared with computational fluid dynamics numerical modelling. Dimethylcadmium and diisopropyltelluride were used as the reactants, released from a recently developed coating head orientated above the glass substrate (of area 15 × 15 cm^2). Depositions were performed in static mode and dynamic mode (i.e., over a moving substrate). The deposited CdTe film weights were compared against the calculated theoretical value of the molar supply of the precursors, in order to estimate material utilisation. The numerical simulation gave insight into the effect that the exhaust's restricted flow orifice configuration had on the deposition uniformity observed in the static experiments. It was shown that > 59% of material utilisation could be achieved under favourable deposition conditions. The activation energy determined from the Arrhenius plot of growth rate was ~ 60 kJ/mol and was in good agreement with previously reported CdTe growth using metalorganic chemical vapour deposition (MOCVD). Process requirements for using a chamberless environment for the inline deposition of compound semiconductor layers were presented.

Keywords: CFD modelling; chamberless inline process (CIP); MOCVD; cadmium telluride

1. Introduction

The growth rate of thin-film Cadmium Telluride (CdTe) using metalorganic chemical vapour deposition (MOCVD) has been found to be sensitive to both substrate temperature and reactant partial pressures [1], presenting a complex transport and kinetic process. Among the various deposition techniques used for CdTe growth, MOCVD is a favourable method, allowing control of the microstructure and stoichiometry of the films [2–4]. MOCVD is an attractive method for depositing CdTe and another group II-VI compound semiconductor thin films [5,6]. It has been conventionally associated with a low-pressure batch process for the fabrication of optoelectronic devices [7], including multi-junction III-V photovoltaic cells for space applications [8]. Physical vapour deposition (PVD) techniques, such as closed-space sublimation (CSS) [9] or vapour transport deposition (VTD), are more commonly used for the deposition of thin-film CdTe for photovoltaic (PV) applications. For example,

First Solar has achieved a low production cost of ~$0.49 per watt using VTD for commercial CdTe PV modules [10], whereas the efficiency has been increased to 21%, as reported by Green et al. [11]. Since PVD techniques are generally associated with vacuum processing, an alternative non-vacuum and scalable deposition processes, such as chamberless MOCVD, are desirable. Material utilisation of 40% for MOCVD of CdTe and conversion efficiency exceeding 11% for the fabricated CdTe solar cell devices have already been demonstrated using an inline reactor design [12,13].

Gas flow behaviour has a significant impact on the uniformity and reproducibility of coatings produced by MOCVD. In a previous paper, we reported the modelling of a vertical low-pressure MOCVD reactor geometry [14], providing an understanding of the film growth mechanism and complex chemical reactions.

Our group used computational fluid dynamics (CFD) modelling in the development of the coating head [15] for the chamberless coating setup described in the present paper. In a precursor to the work reported in this paper, Yang et al. [16] conducted three-dimensional (3D) simulations using CFD code – Fluent, investigating the effects of various conditions on CdTe film growth in an inline MOCVD reactor, where precursor gas flows were delivered normally to the direction of substrate translation. There, the sequential reactions involved in the CdTe deposition process were significantly simplified by the adoption of a proposed global surface reaction.

This paper focused on two aspects of our chamberless inline MOCVD process: (1) the influence and optimisation of the exhaust restricted flow orifice (RFO) configuration, related to the deposition profile in static mode (i.e., on a stationary substrate), and (2) the effects of key deposition parameters on the pyrolysis of CdTe in the dynamic mode (i.e., on a moving substrate), including substrate temperature (T_s), precursor concentration (P_{con}) and total gas flow (F_{total}). The deposition profiles, measured film thicknesses and material (chemical precursor) utilisation were correlated to CFD simulations.

2. Experimental Section

The experiments were carried out using a chamberless inline system, incorporating 6 individual coating heads capable of depositing different materials by MOCVD [17]. A single coating head on this system was used to deposit the CdTe layers reported in this work. Precursor gas flows were released from the coating head normal to the glass substrate being deposited on. The coating head consists of a precursor delivery system, surrounded by containment curtain flows (CCF) and a balanced flow exhaust system, which is pressure and flow controlled by a combination of regulated extraction and individual RFOs positioned around the deposition zone of the coating head [15]. Figure 1 shows a projection view of these components in the plane of substrate deposition, along with Figure 2 showing the over-layer grid system used for the analysis of deposition characteristics in static and dynamic modes. The chemical precursors used were dimethylcadmium (DMCd) and diisopropyltelluride (DIPTe) for cadmium (Cd) and tellurium (Te), respectively. High purity hydrogen (H_2) gas (99.995%) was used for the main carrier gas, and nitrogen (N_2) gas (99.9995%) was used for CCF. The heated stage was motion controlled and able to be positioned under any 1 of the 6 coating heads. Heating was achieved through infrared quartz elements radiating toward a graphite susceptor upon which the glass sample was mounted. The stainless steel surface temperatures of the coating head and the heated stage were maintained at 20–30 °C by using a closed-loop water cooling system. The temperature on the substrate's surface corresponded to the average surface temperature measured during temperature calibration (Figure 3). The set-point temperature from the controller was compared with the averaged measured substrate surface temperature (from 3 different areas) and was within ±10 °C over a 15 × 15 cm^2 area centrally located on the heated zone.

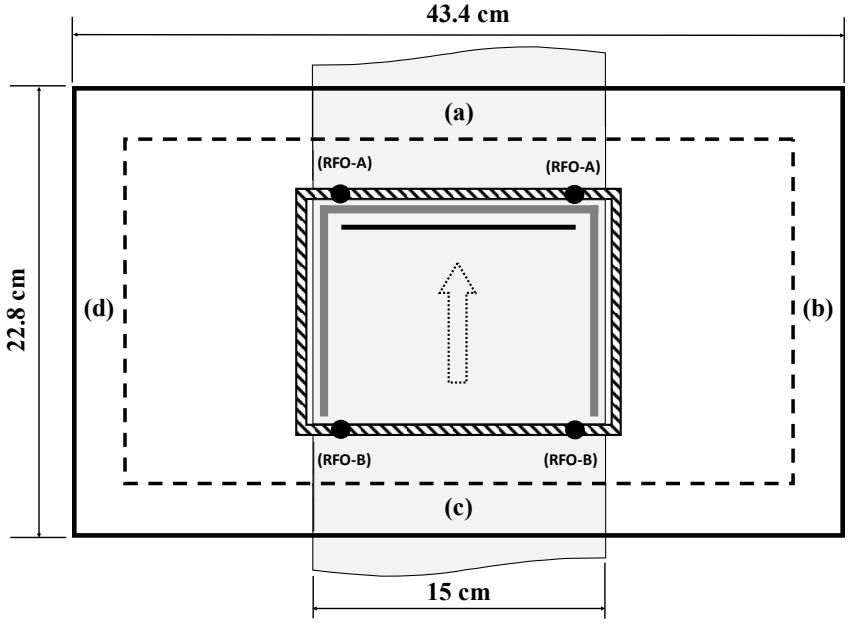

Figure 1. Schematic representation of the coating head components [15]. The dashed edges (**a–d**) represent the containment curtain flows (CCF), the single solid line represents the precursor delivery, the dark solid grey shaded line represents the flow guide plate, the hashed square represents the active exhaust, surrounding the deposition area, and the black dots (RFO-A and RFO-B) represent the extraction points. The discontinuous light grey band represents the substrate width, while the central arrow indicates the direction of travel [17]. RFO: restricted flow orifice. Reproduced with permission from MOCVD for solar cells, a transition towards a chamberless inline process; published by Elsevier, 2015.

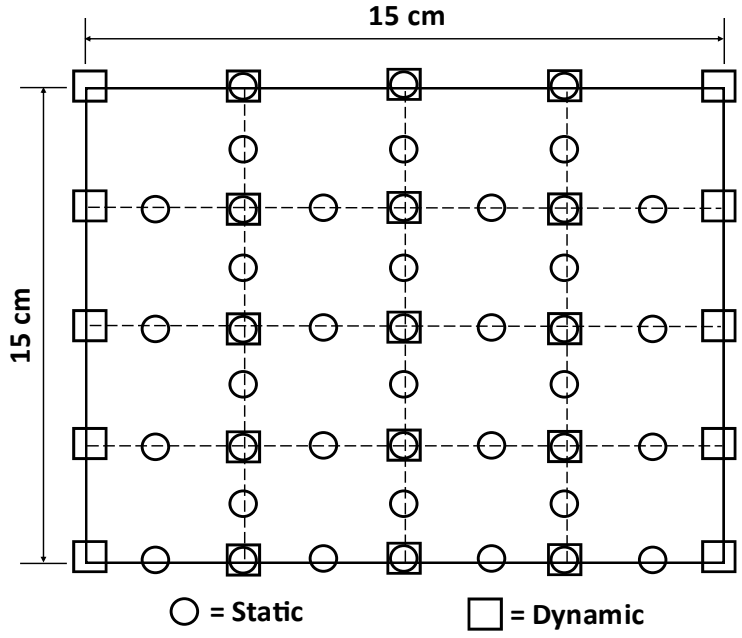

Figure 2. Schematic representation of the over-layer grid system used for analysis on the substrate plane. Note that the dashed line is the "over-layer grid system" and only a guide to the eye for the profilometry measuring points.

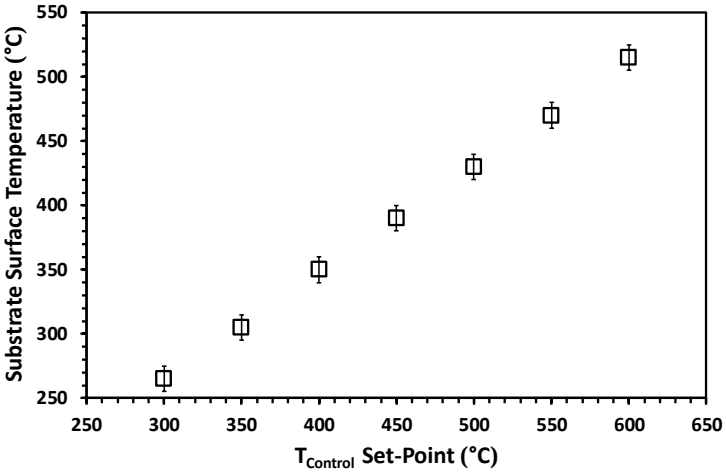

Figure 3. Controller temperature set-point vs averaged measured substrate surface temperature.

CdTe layers were deposited on 3 mm thick 20 × 30 cm^2 Neoceram^{TM} (Ceramic Glass Ltd., Loughborough, England) type glass rectangles for static mode operation. The area and coverage of the deposited (A_{dep}) layers were assessed over the central 15 cm × 15 cm area using the over-layer grid system shown in Figure 2 (static), by which any spread in the deposited film thickness and the deposited volume (v_{exp}) of the material was determined. The material utilisation (Uv_{mat}) was calculated using Equation (1).

$$Uv_{mat} = \frac{v_{\exp}}{v_{theor}} \times 100\% \quad (1)$$

where v_{exp} was calculated using:

$$v_{\exp} = d \times A_{dep} \quad (2)$$

where d is the average film thickness, A_{dep} is the deposited area, v_{theor} is the theoretical volume of CdTe deposit, limited by the molar supply of the metal-organic precursor [10], which was calculated using the relationship

$$v_{theor} = \frac{p_{mo} F_{mo} t_d N_A}{22.4} \times \frac{a_0^3}{4} \quad (3)$$

where p_{mo} and F_{mo} are the partial pressures and the mass flow rate, respectively, of the limiting precursor (DiPTe in this series of experiments), t_d is the deposition time, N_A is the Avagadro constant, a_0 is the lattice constant of CdTe (6.48 Å). The RFO diameters were varied from 0.5 to 1.0 mm, and the differential pressure of the active exhaust was controlled from −5 to −15 Torr (relative to ambient pressure).

For the dynamic mode experiments, CdTe layers were deposited on 3.2 mm thick 15 × 15 cm^2 TEC^{TM} C15 glass substrates provided by NSG Pilkington (Nippon Sheet Glass Co Ltd., Mita Minato-ku, Tokyo), moving at a translation speed (v_{sub}) of 1.8 cm/min. The mass deposit ($m_{\exp}$) and d were measured from a 5 × 5 cm^2 specimen cut out from the centre of the substrate after deposition, due to the size restriction on the micro-balance used. The material utilisation based on gravimetric measurements (Uw_{mat}) was calculated from:

$$Uw_{mat} = \frac{m_{\exp}}{m_{theor}} \times 100\% \quad (4)$$

The resolution of the measured mass $m_{\exp}$ was 0.1 mg (micro-balance resolution). The theoretical mass (m_{theor}) of the deposit was calculated using:

$$m_{theor} = v_{theor} \times \rho_{CdTe} \quad (5)$$

with ρ_{CdTe} being the density of CdTe (5.86 g/cm^3 at 25 °C) [18]. In these experiments, the deposition surface temperature (T_s) was varied between 305 °C and 470 °C, the precursor concentrations (i.e., partial pressures) were varied from 1.38 to 3.48 Torr for DMCd and 0.44 to 1.08 Torr for DiPTe, and F_{Total} from 0.5 to 1.0 L/min.

The layer thicknesses in static and dynamic modes were measured using a Veeco Dektak 150 (Veeco Instruments Inc. Planview, New York, United Staes) stylus profilometer over the available data points (Figure 2). The dynamic growth rates (GR) given were determined using the averaged final thickness in relation to the time of deposition, t_d (i.e., duration of substrate passing through the active deposition zone).

3. Numerical Modelling

Simplified 2D and 3D models of the coating head delivery system were developed, using a combined mesh not exceeding 100,000 cells for 2D and 700,000 cells for 3D to define the numerical model. In order to correlate simulation with experimental data, a surface chemical reaction was applied for the 2D model for simplification. The 3D model employed H_2 and N_2 as the mass species, presenting the deposition profile of H_2 on the substrate, determined by the CCF, RFO configuration and active exhaust extraction. A finer mesh, in the vicinity of the substrate, was employed to account for the influence of the temperature gradient and boundary layer formation. A no-slip boundary condition was prescribed on the domain walls, the exit of the system (i.e., exhaust) was defined as outflow, while the velocity out of the injector was defined as inlet velocity (i.e., based on total flow rate). In addition, any experimental apparatus walls that were controlled by water cooling were approximated as isothermal walls within the numerical models. A constant temperature condition was applied to the substrate surface. Pressure-velocity coupling was obtained using the SIMPLE [19] algorithm, with the discretisation scheme for pressure being second-order. To ensure stability, the momentum, energy and chemical species transport were set to first-order upwind. In order to derive the differential equations for expressing conservation of mass, momentum and energy, some assumptions were made: (1) the gas mixture is a continuum; (2) gas flows are laminar; (3) steady-state conditions prevail; (4) the equation of state obeys the ideal gas law. Under these assumptions, the differential equations were simplified as by Yang et al. [16]. Further, due to the lack of detailed chemical data regarding the deposition of CdTe thin film from the gas mixture, one overall surface chemical reaction on the substrate was considered [16]:

$$DIPTe(g) + DMCd(g) + H_2 \rightarrow CdTe(s) + Res(g) \quad (6)$$

where $Res(g)$ represents all the by-products of the reaction. The following Arrhenius expression was used to express the rate of the reaction:

$$k = AT^{\beta}e^{-\frac{E_a}{RT}} \quad (7)$$

where A is the pre-exponential factor, which relates to the reaction frequency between the precursor molecules, E_a is the activation energy to initiate the reaction, R is the universal gas constant (8313 J/K·mol) and β is the temperature exponent. The pre-exponential factor was set to $A \approx 1016$ s^{-1} [20], the temperature exponent β was set to 0 and the activation energy E_a was set to 59.62 kJ·mol^{-1}.

All simulations were conducted on a Fujitsu Celsius W510 ProGREEN workstation, with a Quad-Core Intel Xenon, 3.3 GHz and 16.0 GB RAM, running the commercial CFD software ANSYS Fluent (ANSYS, Canonsburh, PA, USA).

4. Results and Discussion

4.1. Static Mode – Deposition Profile

A series of CdTe thin films were grown with t_d = 20 min, T_s = 430 °C and F_{Total} = 0.5 L/min. In order to study the deposition profile behaviour, the RFO sizes and active exhaust were varied, as shown in Table 1.

Table 1. Parametric variables for static mode (locations of RFO-A and RFO-B are shown in Figure 1).

Configuration	RFO Size (mm)		Active Extraction
	(RFO-A)	(RFO-B)	(Torr)
S-1	0.5	0.7	−10
S-2	0.7	0.5	−10
S-3	0.7	0.5	−15
S-4	1.0	0.5	−10

RFO - Restricted Flow Orifice.

The deposition profiles shown in Figure 4 highlighted that thin-film growth was strongly dependent on the RFO configuration. The change in the active exhaust from −10 to −15 Torr (S-2 to S-3) had very little impact on the material utilisation when compared with S-2. From CFD simulations, the velocity profile was obtained 8 mm upstream and downstream of the injector slit (Figure 5a). The configuration of RFOs in S-1 resulted in a greater flow direction downstream of the injector due to the extraction being stronger with 0.7mm and 0.5mm RFOs in situ for RFO-A and RFO-B, respectively. However, by alternating the configuration, as in S-4, reduced the extraction strength downstream, resulting in a recirculating vortex located behind the injector slit and in front of the flow guide plate. The film thickness (d) data for the extreme cases (S-1 and S-4), presented in Figure 5b, confirmed that the deposited profile was narrower and the peak (maximum) film thickness was greater with S-4. This was expected to be related to the vortex generated near the flow guide plate compared with S-1, as seen in Figure 6a,b. Figure 6 only shows the exhaust located behind the injector RFO-A, the guide flow plate was located in this section and had a direct influence on the overall deposited layer due to the presence of the recirculating vortex in S-4 RFO configuration. The downstream extraction point (RFO-B) had no direct influence or change in the fluid flow pattern and, therefore, only this exhaust is presented in Figure 6. The vortex provided an alternative route to increase residence time on the surface of the substrate for the unreacted precursors to be recycled, therefore, increasing the material utilisation, as shown in Figure 7. However, due to the recirculating vortex, the overall uniformity of the deposited layer was affected with such configuration. Therefore, S-1 configuration was chosen for dynamic mode analysis, depositing a larger uniform surface area.

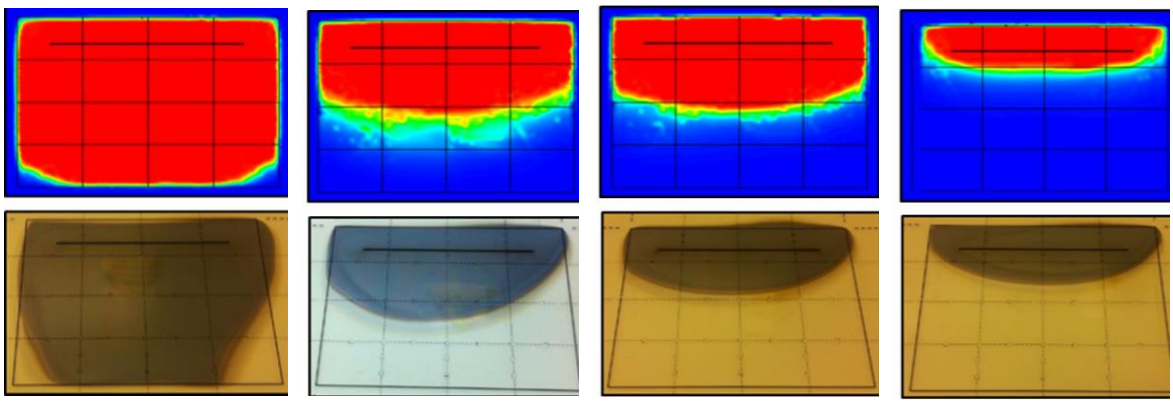

(**a**) (**b**) (**c**) (**d**)

Figure 4. Cadmium Telluride (CdTe) static deposition profiles from experimental samples (bottom) and computational fluid dynamics (CFD) simulations (top). Deposition conditions varied from S-1 (**a**) to S-4 (**d**) in sequence, as given in Table 1.

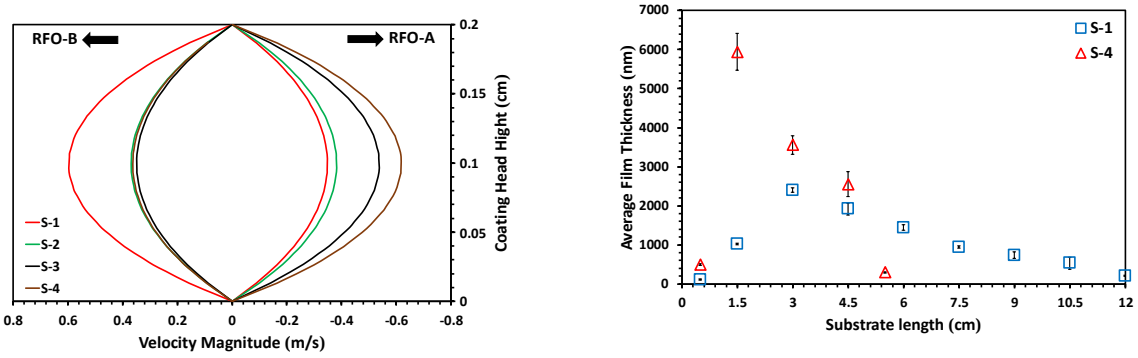

(**a**) (**b**)

Figure 5. (**a**) Flow velocity profile (m/s) 8 mm in the front and behind the precursor injector slit for S-1–S-4 configurations. (**b**) Mapping of CdTe film thickness profiles obtained in static mode for deposition conditions S-1 and S-4.

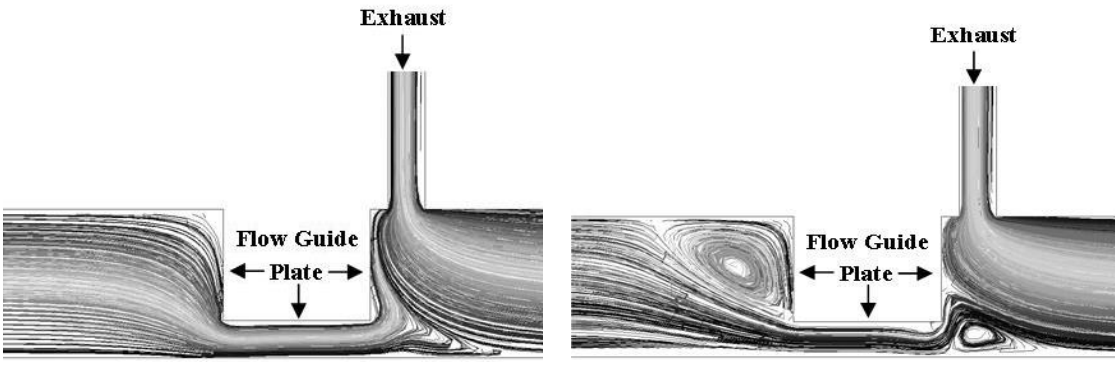

(**a**) (**b**)

Figure 6. Path lines located behind the precursor injector slit (i.e., near RFO-A in Figure 1) around the flow guide plate and the exhaust (**a**) for S-1 and (**b**) for S-4.

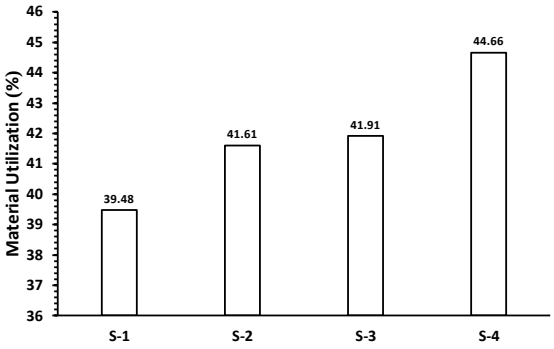

Figure 7. Material utilisation calculated using (1) for S-1–S-4 configurations.

4.2. Dynamic Mode – Deposition Kinetics

A series of CdTe thin films were grown using the S-1 configuration, with F_{Total} = 1.0 L/min and v_{sub} = 1.8 cm/min, where only T_s was varied in order to correlate the kinetic regime of the pyrolysis of CdTe layer with CFD simulations (Figure 8a). The activation energy (E_a) of the surface kinetic reaction was calculated from Equation (8) using the linear range from the Arrhenius plot in Figure 8a.

$$\ln(GR) = \ln(A) - \frac{E_a}{RT_s} \tag{8}$$

where GR is the growth rate, and R is the gas constant (8.314 J/K·mol).

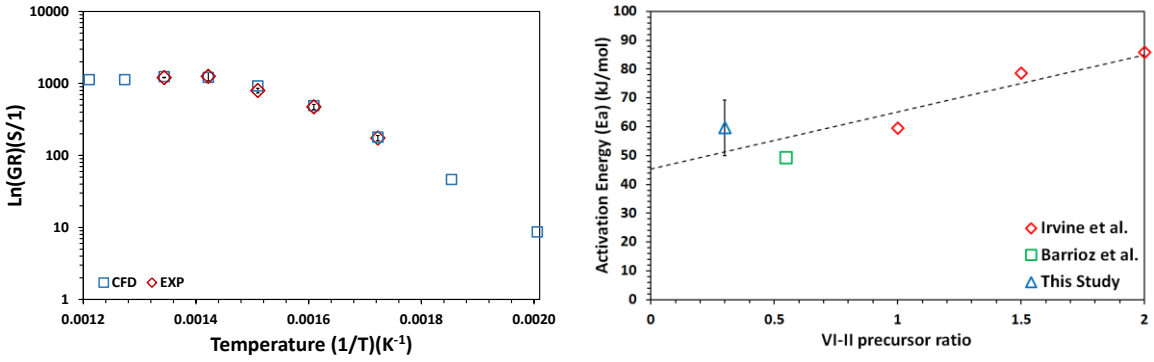

(**a**) (**b**)

Figure 8. Using the S-1 configuration for the chamberless coating head during the deposition of CdTe, results are displayed as (**a**) an Arrhenius plot of ln(GR) vs 1/T used to calculate the activation energy and (**b**) a VI:II precursor ratio vs activation energy. GR: growth rate.

Saturation of GR was observed for T_s > 420 °C; therefore, the linear region in the lower temperature range was used to calculate E_a, with a value of 59.62 kJ/mol. This appeared to be somewhat larger than the results experimentally obtained by Barrioz et al. [12] (49 kJ/mol) for a slightly larger VI:II precursor ratio for deposition in an enclosed inline MOCVD reactor (Figure 8b). Barrioz et al. [12] also observed saturation in GR at higher temperatures (i.e., >405 °C), attributed to mass transport limitation due to the Te precursor's concentration. Despite the slightly higher activation energy, the activation energy as a function of VI:II ratio followed the trend observed by previous authors [12,21] within experimental errors.

Using the S-1 configuration, a series of CdTe thin films were grown for F_{Total} = 0.5 L/min and F_{Total} = 1.0 L/min while maintaining the precursor partial pressures constant at DMCd = 3.48 Torr and DIPTe = 1.08 Torr, v_{sub} = 1.8 cm/min, while varying T_s (Table 2).

Table 2. Layer thickness and material utilization as a function of T_s from 305 °C to 470 °C for F_{total} = 0.5 L/min and F_{total} = 1.0 L/min.

Total Flow (L/min)	T (°C)	Exp (d) (μm)	CFD (d) (μm)	Exp (Uw_{mat}) Avd (%)	Exp (Uw_{mat}) Stdv (%)	Exp (Uv_{mat}) Avd (%)	Exp (Uv_{mat}) Stdv (%)	CFD (Uv_{mat}) (%)
0.5	225	-	0.018	-	-	-	-	1.47
	265	-	0.066	-	-	-	-	5.42
	305	0.172	0.178	18.56	0.30	14.20	0.47	14.71
	350	0.339	0.359	28.12	0.29	27.94	0.88	29.60
	390	0.450	0.533	38.11	0.31	37.10	1.81	43.98
	430	0.598	0.621	50.90	0.31	49.32	0.39	51.17
	470	0.634	0.626	39.29	0.35	52.29	0.21	51.67
	515	-	0.604	-	-	-	-	49.88
	555	-	0.538	-	-	-	-	44.43
1.0	225	-	0.009	-	-	-	-	0.36
	265	-	0.046	-	-	-	-	1.92
	305	0.175	0.180	7.34	0.30	7.22	0.51	7.42
	350	0.474	0.493	18.20	0.29	19.56	1.58	20.36
	390	0.799	0.926	29.30	0.32	33.56	2.48	38.24
	430	1.257	1.213	45.80	0.30	51.91	7.20	50.10
	470	1.209	1.248	45.70	0.38	49.94	0.47	51.56
	515	-	1.130	-	-	-	-	46.66
	555	-	1/133	-	-	-	-	46.80

Total Flow – precursor total flow; T – substrate temperature. Exp (d) – experimental layer thickness; CFD (d) – numerical layer thickness; Exp (U_{Wmat}), Exp (U_{Vmat}) – experimental results for material utilization; Avd – averaged results; Stdv – standard deviation; CFD (U_{Vmat}) – numerical results for material utilization.

The deposited layers were further examined for CdTe characterisation. The elemental analysis of the CdTe layers was conducted using energy dispersive X-Ray (EDX) spectroscopy analytical technique; Figure 9a presents the elemental composition of the measured specimen. Furthermore, scanning electron microscopy (SEM) presented in Figure 9b shows the surface topography and grain structure of the deposited layer. The utilisation of CdTe layer grown using the chamberless inline deposition system has been achieved by Kartopu et al. [13] in a photovoltaic solar cell device and obtaining device results comparable with horizontal (tube) MOCVD batch reactor.

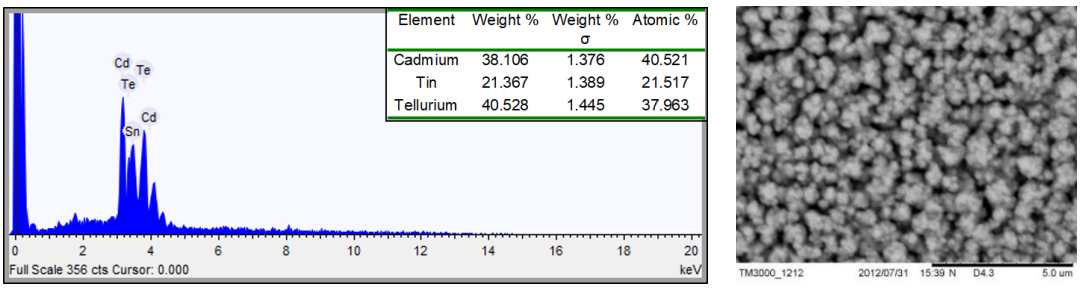

(**a**) (**b**)

Figure 9. Material characterisation of deposited CdTe using the S-1 configuration for the chamberless coating head; results are displayed as (**a**) EDX result, presenting an elemental composition of the measured sample, and (**b**) SEM results, showing the surface topology and grain structure of CdTe deposited layer.

From Table 2, it is clear that both the film thickness and material utilisation were increased with T_s up to ~ 470 °C; however, a plateau was reached for higher temperatures. In relatively low T_s regime, ranging from 305 °C to 420 °C, the deposition of CdTe was strongly dominated by a second-order kinetic regime. Above 420 °C, the material utilisation reached a plateau at 50–60%, related to a mass

transport limited regime; further study of the fluid dynamics would provide potential to reach higher usage of the precursors. The gravimetric measurements from Table 2 provided the most reliable values, considering that they were less influenced by non-uniformity in thickness. The variations between experimental and simulated data could be attributed to the fact that CFD modelling uses a simplified environment and chemical reaction (Equation (6)). Further increase of T_s above 500 °C reduced material utilisation, which could be attributed to desorption of tellurium species from the growth surface, as calculated from CFD modelling (Table 2) and previously observed by Irvine et al. [21].

Material utilisation of 50%–60% could be reproducibly achieved when the pyrolysis of CdTe takes place at temperatures between 430 °C and 470 °C, as could be seen from Table 2. It is expected that the residence time of precursors on the substrate surface could be further improved, leading to higher material utilisation; this would be the subject of further investigation. At higher gas flow, the precursor material utilisation is maintained whilst doubling the film thickness. Overall, the presented results indicated that the use of smaller total flows (at fixed precursor concentrations) was more beneficial in regards to high efficiency in material consumption (Figure 10).

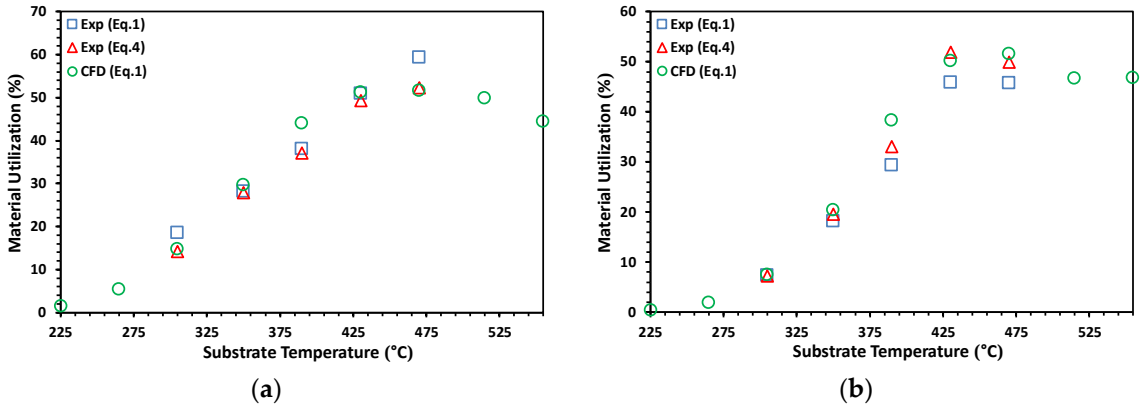

Figure 10. Experimental and numerical comparison of material utilisation as a function of T_s for (**a**) F_{total} = 0.5 L/min and (**b**) F_{total} = 1.0 L/min.

5. Conclusions

Deposition of CdTe layers using a chamberless inline MOCVD process at atmospheric pressure was investigated. The substrate coverage, layer thickness and material utilisation were studied as a function of deposition parameters in both static and dynamic modes. It was shown that the deposition profile was dependent on the active exhaust parameters where the best substrate coverage was obtained using condition S-1. However, the S-4 condition yielded a 12% increase in material utilisation (Figure 7), having the potential to reach ~67% in material utilisation. The study also examined mass transport limited and kinetic regimes with temperatures ranging from 305 °C to 430 °C. It was shown that material utilisation of 60% could be achieved with the potential to reach ~70%. Material utilisation was strongly affected by the deposition temperature and plume control. The activation energy was found to be 59.62 kJ/mol, in reasonable agreement with previously reported values obtained using MOCVD of CdTe for the same precursors but in closed chambers. The numerical CFD modelling correlated well with experimental data regarding the deposition profiles, film thickness and the efficiency of precursor usage. The CFD simulation of CdTe might, therefore, facilitate the control and optimisation in the scaling up of the chamberless inline process (CIP) for thin film deposition.

From the results presented here, it was also notable that the CIP could improve material utilisation for CdTe deposition compared with closed chamber MOCVD batch processes. The scalability and high material utilisation efficiency of CIP offered an alternative process technology for high throughput fabrication of thin-film PV modules.

Author Contributions: Conceptualisation, S.M., V.B. and S.J.C.I.; methodology, G.K.; software, S.M. and X.Y.; validation, S.M.; formal analysis, G.K., V.B., D.L., S.J.C.I. and X.Y.; investigation, S.M., G.K., V.B., D.L., S.J.C.I. and X.Y.; writing—original draft preparation, S.M. and Y.V.; writing—review and editing, S.M. and Y.V.; visualisation, G.K.; supervision, V.B., D.L., S.J.C.I., X.Y. and Y.V. All authors have read and agreed to the published version of the manuscript.

Funding: This research was funded by the European Regional Development Fund through the Low Carbon Research Institute Programme (WEFO-80366) for the Solar Photovoltaic Academic Research Consortium (SPARC) Cymru project and by the European Social Fund project (case ID 80300) for a Knowledge Economy Skills Scholarship (KESS).

Acknowledgments: The authors would like to thank ESF and MD Ian Owen from Scanwel Ltd. for funding the Knowledge Economy Skills Scholarship (KESS) and the Low Carbon Research Institute (LCRI) for funding the SPARC project. Paul Warren, from NSG Pilkington, is also thanked for supplying the TEC glass for the SPARC project and Design Engineer Steve Truman from Scanwel Ltd. for the design and assembly of the coating heads. The authors would also like to thank Peter Siderfin and Steve Jones, CSER, for their help in the commissioning of the SPARC inline deposition system. Damien Jones and Julien Haillet are also acknowledged for their contributions to the PLC programming on the system.

Conflicts of Interest: The authors declare no conflict of interest.

References

1. Lee, Y.H.; Chou, K.S.; Lin, M.S. Analysis of the combined effect of mass transfer and decomposition kinetics on the growth rates of CdTe by MOCVD. *J. Chin. Inst. Eng.* **1988**, *11*, 551–554. [CrossRef]
2. Piotrowski, A.; Madejczyk, P.; Gawron, W.; Klos, K.; Pawluczyk, J.; Grudzien, M.; Piotrowski, J.; Rogalski, A. Growth of MOCVD HgCdTe heterostructures for uncooled infrared photodetectors. *Bull. Pol. Acad. Sci. Tech. Sci.* **2005**, *53*, 139–149. [CrossRef]
3. Kartopu, G.; Phillips, L.J.; Barrioz, V.; Irvine, S.J.C.; Hodgson, S.D.; Tejedor, E.; Dupin, D.; Clayton, A.J.; Rugen-Hankey, S.L.; Durose, K. Progression of metalorganic chemical vapour-deposited CdTe thin-film PV devices towards modules. *Prog. Photovolt. Res. Appl.* **2016**, *24*, 283–291. [CrossRef]
4. Luceno-Sanchez, J.A.; Diez-Pascual, A.M.; Capilla, R.P. Materials for photovoltaics: State of art and recent developments. *Int. J. Mol. Sci.* **2019**, *20*, 976. [CrossRef] [PubMed]
5. Mullin, J.B.; Irvine, S.J.C.; Ashen, D.J. Organometallic growth of II–VI compounds. *J. Cryst. Growth* **1981**, *55*, 92–106. [CrossRef]
6. Hicks, R.F. The chemistry of the organometallic vapor-phase epitaxy of mercury cadmium telluride. *Proc. IEEE* **1992**, *80*, 1625–1640. [CrossRef]
7. Moon, R.L. MOVPE: Is there any other technology for optoelectronics? *J. Cryst. Growth* **1997**, *170*, 1–10. [CrossRef]
8. Rushworth, S. High purity metal-organic precursors for CPV device fabrication. *Mater. Matters* **2010**, *5*, 94–98.
9. McCandless, B.E.; Sites, J.R. Cadmium telluride solar cells. In *Handbook of Photovoltaic Science and Engineering*, 2nd ed.; Luque, A., Hegedus, S., Eds.; Wiley: Chichester, UK, 2012; pp. 600–642.
10. First Solar Hits Cost Reduction Milestone. Available online: https://www.pv-tech.org/news/has_first_solar_retaken_the_lowest_cost_pv_manufacturer_mantle (accessed on 13 December 2019).
11. Green, M.A.; Hishikawa, Y.; Dunlop, E.D.; Levi, D.H.; Hohl-Ebinger, J.; Yoshita, M.; Ho-Baillie, A.W.Y. Solar cell efficiency tables (Version 53). *Prog. Photovolt. Res. Appl.* **2019**, *27*, 3–12. [CrossRef]
12. Barrioz, V.; Kartopu, G.; Irvine, S.J.C.; Monir, S.; Yang, X. Material utilisation when depositing CdTe layers by inline AP-MOCVD. *J. Cryst. Growth* **2012**, *354*, 81–85. [CrossRef]
13. Kartopu, G.; Barrioz, V.; Irvine, S.J.C.; Clayton, A.J.; Monir, S.; Lamb, D.A. Inline atmospheric pressure metalorganic chemical vapour deposition for thin film CdTe solar cells. *Thin Solid Film.* **2014**, *558*, 374–377. [CrossRef]
14. Mitrovic, B.; Gurary, A.; Quinn, W. Process conditions optimisation for the maximum deposition rate and uniformity in vertical rotating disc MOCVD reactors based on CFD modelling. *J. Cryst. Growth* **2007**, *303*, 323–329. [CrossRef]
15. Barrioz, V.; Lamb, D.A.; Monir, S.; Trueman, S.; Kartopu, G.; Owen, I.W.; Irvine, S.J.C.; Yang, X. Injector and Method. Patent WO2014122484A1, 14 August 2014.

16. Yang, X.; Wu, Y.; Huang, X.; Barrioz, V.; Kartopu, G.; Monir, S.; Irvine, S.J.C. Numerical simulation of the deposition process and the epitaxial growth of cadmium telluride thin film in a MOCVD reactor. *Comput. Therm. Sci.* **2013**, *5*, 177–188. [CrossRef]
17. Barrioz, V.; Monir, S.; Kartopu, G.; Lamb, D.A.; Brooks, W.; Siderfin, P.; Jones, S.; Clayton, A.J.; Irvine, S.J.C. MOCVD for solar cells, a transition towards a chamberless inline process. *J. Cryst. Growth* **2015**, *414*, 223–231. [CrossRef]
18. Capper, P. *Properties of Narrow Gap Cadmium-Based Compounds*; IEE: London, UK, 1994.
19. Fluent Inc. *Fluent 6.3 UDF Manual*; Fluent Inc.: Lebanon, PA, USA, 2006.
20. Mazi, M.; Simka, H.; Jensen, K.F. Simulation of carbon doping of GaAs during MOVPE. *J. Cryst. Growth* **1992**, *124*, 483–492.
21. Irvine, S.J.C.; Bjaj, J. A study of the growth kinetics of II–VI metalorganic vapour phase epitaxy using in situ laser reflectometry. *J. Cryst. Growth* **1994**, *145*, 78–81. [CrossRef]